Chemistry Research Journal, 2018, 3(6):76-81

Available online www.chemrj.org

Research Article

ISSN: 2455-8990
CODEN(USA): CRJHA5

Properties of Nano Hydroxyapatite Powder Derived from Human Teeth

Kerim Emre ÖKSÜZ

Sivas Cumhuriyet University, Department of Metallurgical & Materials Eng., 58140, Sivas, Turkey

Abstract Tooth enamel, the hardest tissue in the human body, is composed mainly of calcium phosphate mineral crystals which has a chemical formula $Ca_{10}(PO_4)_6(OH)_2$ (HA, hydroxyapatite). Understanding the various properties of human teeth and dental materials is the basis for the development of restorative materials. The production of nano hydroxyapatite powder derived from human teeth was studied in this paper. The nano hydroxyapatite powder (≈ 52 nm) was produced by calcination without compaction. The dried and calcined powder were characterized for phase composition using X-ray diffractrometry, Fourier transform infrared spectroscopy and Energy-*dispersive* X-ray *spectroscopy techniques*. The average crystallite size of HA powder was calculated by Debye Scherrer's formula. Field emission scanning electron microscopy and Transmission electron microscopy studies were performed for further investigation of particle size and powder morphology.

Keywords Nano-powder, characterization, hydroxyapatite, teeth, biomaterials

1. Introduction

Hydroxyapatite (HA) which has a Ca/P ratio of 1.667 with a chemical formula of $Ca_{10}(PO_4)_6OH_2$has achieved the most significant attention because of its compositional similarities to the natural human bone and teeth, and its excellent biocompatibility[1]. HA has a hexagonal crystallographic structure with a space group, P63/m. This space group is characterized by a six-fold *c*-axis perpendicular to three equivalent *a*axes (a_1,a_2,a_3) at angles 120° to each other (see Fig.1).There are two types of HA either synthetic or from natural origin; synthetic HA is the most frequently used, although it is expensive and does not completely match with the human teeth chemical composition, but it is more reliable. On the other hand, the natural HA has an economic advantage, but there are significant concerns about the use of natural HA, due to the potential transmission of dangerous diseases when it is not well prepared [2]. Due to the attractive properties of HA, various techniques have been developed to produce synthetic hydroxyapatite such as wet precipitation [3], sol-gel method [4], hydrothermal synthesis [5] and mechano-chemical method [6]. It can also be synthesized from natural sources such as bovinebones, egg shells, human teeth, coral reefs, etc. [7-9]. In addition, it is reported that nano HA particles have a preventative effect on the proliferation of tumor cells [10]. Apparently different characteristics of HA particles, such as morphology, size and crystallinity, have shown different biological consequences [11]. Human teeth are natural composites which comprise of nano HA rods (smaller than 100 nm) arranged in lamellae and bound to collagen [12]. Due to theirnano size, HA crystals have a very large surface area which enables homogenous resorption by osteoclasts [13]. Hence, synthesizing HA of nano scale is of much interest as biocompatible phase reinforcement in biomedical applications [14]. In the present study, nano HA particles derived from human teeth were prepared, and their properties were investigated.

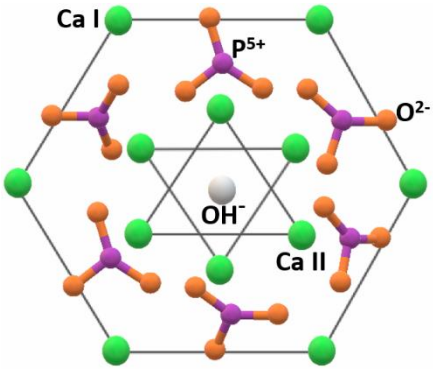

Figure 1: Schematic drawing of one hexagonal building unit of HA [001] direction

2. Experimental Study

In this study the HA material was derived from freshly-extracted human teeth. The teeth samples were obtained from the faculty of dentistry, Sivas Cumhuriyet University, Sivas, Turkey. They were cleaned by boiling to remove organic substances and collagen. Then they were soaked in a 1 % concentration of an antiseptic solution to prevent bad odor and contamination of various infectious diseases. Subsequently they were irrigated again and deproteinized in a 1% NaClO solution. Thereafter, they were calcined at 850°C for 2h with a heating rate of 5°C/min in air. At this temperature, it was observed that organic components were completely burned out and only inorganic phase of calcium phosphate was obtained from dentin and enamel materials. The teeth were crushed into small particles and finally ball milled in isopropyl alcohol using ZrO_2 balls at 300 cycles/min for 144h until fine powder. *Fig. 2 shows* the schematic demonstration of the experimental study.

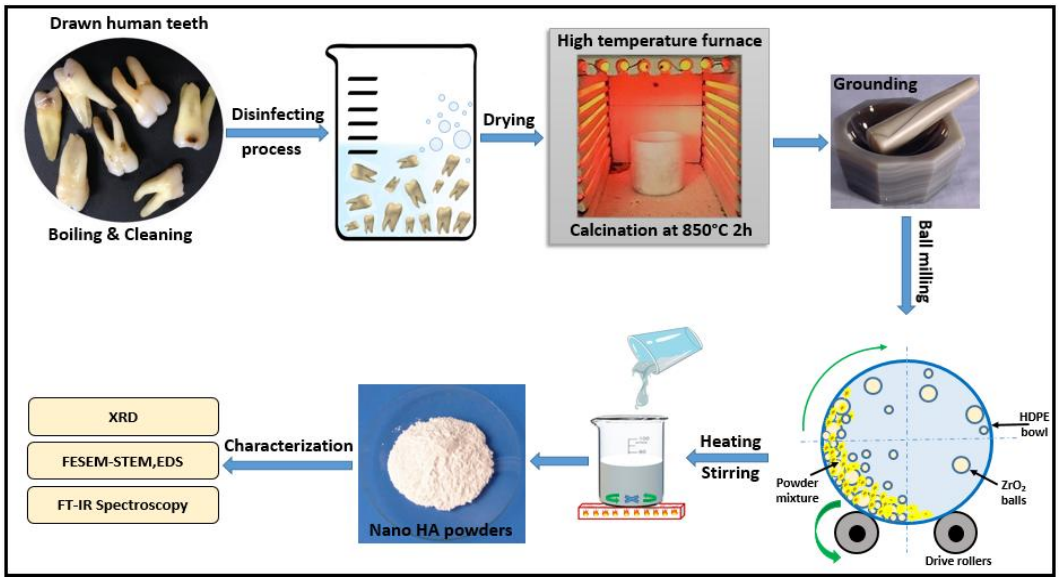

Figure 2: Schematic demonstration of the experimental study

A powder X-ray Diffractometer (Rigaku D/MAX/2200/PC) with a monochromatic Cu-K_α radiation (λ = 1.5408 Å) was used over a 2θ range from 20°to 80° to characterize the crystal structure of the tooth powder, where the diffractograms were compared with the standards complied by the International Centre for Diffraction Data (ICDD).The average crystallite size of the powder was calculated from the XRD line broadening measurement from the Scherrer's equation, [15] which is given by:

$$D = \frac{K\lambda}{\beta cos\theta'} \quad (1)$$

where D is the average crystallite size, λ is the radiation wavelength of Cu-K_{α}, βis the full width at half maximum height of the peak (FWHM), k = 0.9 is the shape factor of the average crystallite and θ is the Bragg angle of the main diffraction peak.

The FT-IR (Bruker Alpha ATR, Germany) was used to determine the chemical function by the wavelength range was up to 4000 cm^{-1} versus the transmittance, the KBr pellets were used as a reference to prevent fluctuations in the output.The chemical elements of calcined powder were analyzed by EDXS(INCA IE 350, and U.K.). The Ca/P ratio was determined by calculating the Ca and P content of the identified compounds containing both elements and compared with the stoichiometric ratio.The microstructure and the surface morphology of the produced powder were observed by field emission scanning electron microscopy (SEM-S-TEM, Tescan Mira 3XMU, Brno, Czechia, 25 kV acceleration voltage, beam current 10 μA) under secondary electron (SE), back scattering (BS) and scanning transmission electron microscope (*S-TEM*) modes, using carbon coated powders. TEM module was mounted onto SEM stage to obtain S-TEM on FE-SEM. The operating voltage was 30 kV and the working distance was adjusted to 3 mm to evaluate the sample on Cu grid more accurately. TEM was on the dark field mode to determine the corresponding layer or particle surfaces with higher contrast.

3. Results and Discussion

3.1. XRD peak analysis

The XRD patterns of the only calcined and, calcined and then ball milled tooth powderare presented in Fig. 3.After ball milling, the some of the sharp peaks were not observed as they might be lost in the background due to broadening as shown in Fig. 3(b). The main crystalline phase, namely Hydroxyapatite – $(Ca_{10}(PO_4)_6(OH)_2$,could be detected in patterns. All the observed peaks were compared with JCPDS file card number (09-0432) for hydroxyapatite and there were small amount of secondary peaks that exist, such as α-TCP and β-TCP in the XRD results. But these small amounts of α-TCPor β-TCP phases could be very helpful at osseointegration. It is known that the calcination of bone/teeth apatite to 800°C yields formation of β-TCP. The HA phase transformation during sintering/calcination consists of two processes: dehydroxylation and decomposition. In dehydroxylation, HA gradually loses OH^- ions at elevated temperature and turns to oxyhydroxyapatite. Dehydroxylation generally contains different stages: at low temperature (800°C), reversible dehydroxylation proceeds at a slow rate. At an intermediate temperature (800–1350°C), reversible dehydroxylation is accompanied by HA decomposition, i.e., HA can decompose into α-calcium phosphate (α-TCP), β-calcium phosphate (β-TCP) and calcium phosphate (CaO) [16,17].

In Fig. 3., It could be observed that the decrease in HA crystallinity and size with the ball milling process. Based on the observation of the XRD pattern, it was noted that the average crystallite size, decreased from 153 nm ±25 to 48 nm ±12, respectively (Fig. 3(a)-Fig. 3(b)).

3.2. FT-IR Study

Fig. 4 shows the FT-IR spectra of the tooth powder calcined at 850°C for 2h. In FT-IR spectra, the bands at 1030 and 1090 cm^{-1}corresponded to the v_3 vibration of PO_4^{3-} ions. The bands at 969 and 1030 cm^{-1}were assigned to the $v_1$vibration of the O–P–O mode and the peaks at 604 and 565 cm^{-1} were attributed to the $v_4$vibration of the O–P–O mode. The weak peaks at 1640 and 1420 cm^{-1} corresponded to absorbed water and vibration of CO_3^{2-}ions content which may exist due to carrying out the experimental procedure under air and therefore the absorption of CO_2 from the atmosphere.The peaks at 1090, 1030, 604 and 565 $cm^{-1}$are characteristic peaks for HA. The bands at 1090 and 565 cm^{-1} corresponded to the v_3 and $v_4$vibration and the vibrational band at 635 cm^{-1} and the stretching band at 3570 cm^{-1} were assigned to structural OH^- of HA. A small peak at 875 cm^{-1} could be attributed to calcium deficient HA [17-19].

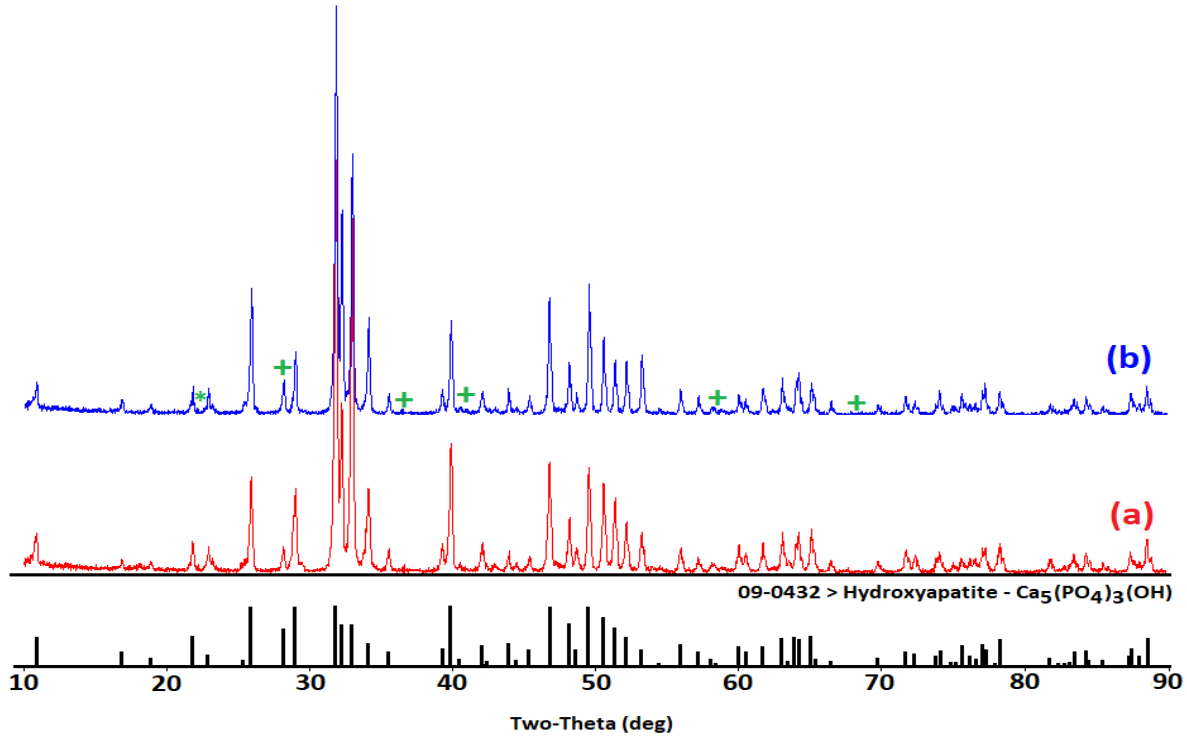

Figure 3: X-ray diffraction patterns of HA powder (a) after calcination, (b) after calcination and ball milling. (*) α-TCP, (+) β-TCP

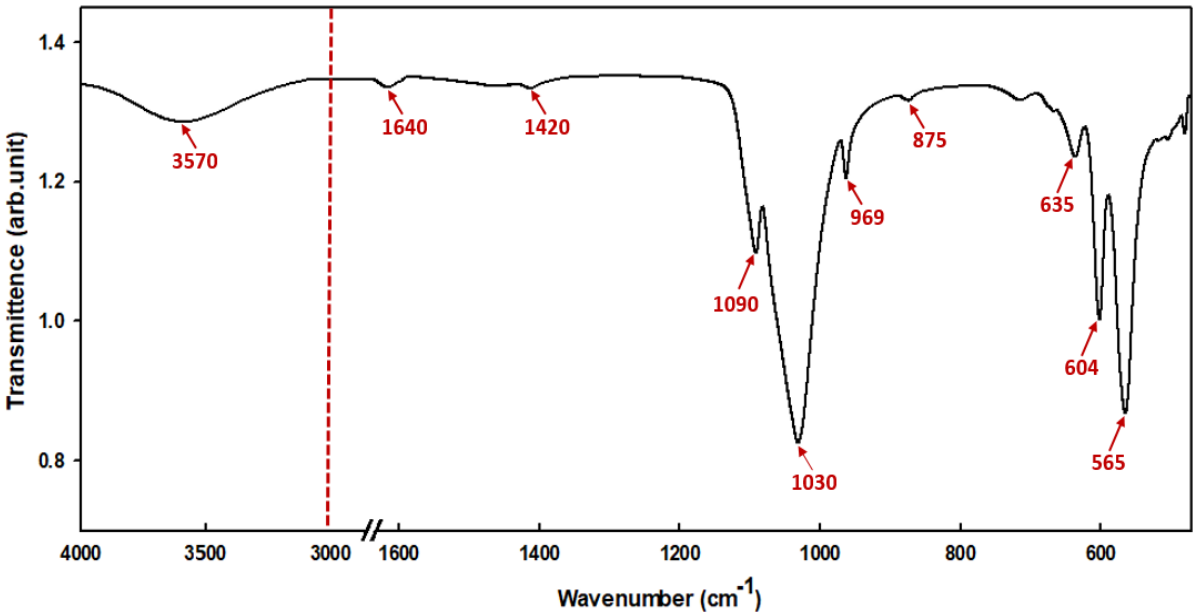

Figure 4: FT-IR spectra of nano HA powder (enlarged view of 3000–4000 cm^{-1} spectra on the left side)

3.3. Microstructural Analysis

Fig. 5(a) and Fig. 5(b) represent the FE-SEM image and EDXS spectra of the tooth powder calcined at 850°C 2h and after ball milling for 144h, respectively. Fig. 5(a) reveals that the homogeneous morphology was obtained for calcined tooth powder after ball milling. EDXS showed the elemental composition of tooth powder as; Na 0.653 %, Mg 0.489 %, P 15.893 %, and Ca 26.510 %. Energy dispersive X-ray spectroscopy results showed a Ca/*P*ratio close to stoichiometric ratios for hydroxyapatite, which is around 1.668 in literature (Fig. 5(b)).

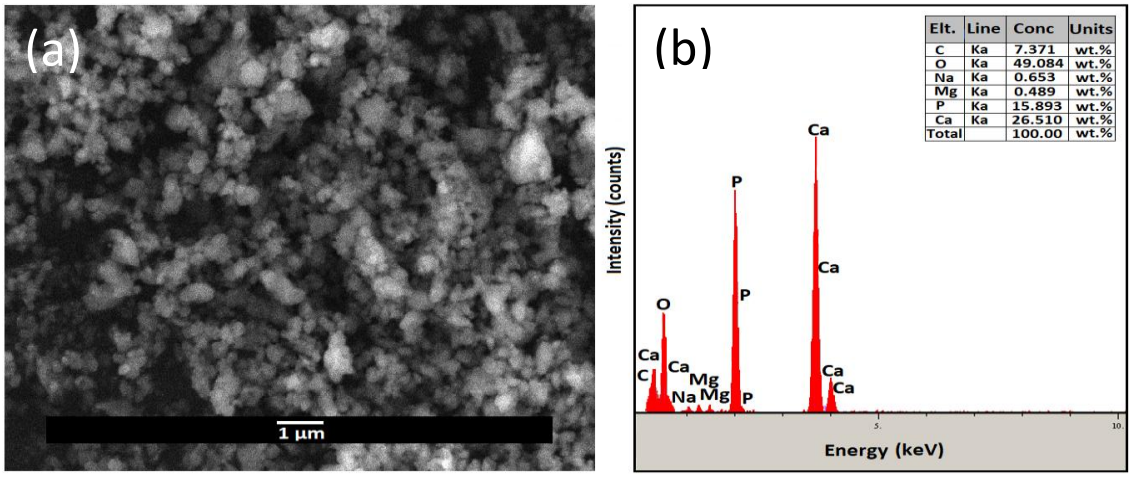

Figure 5: (a) FE-SEM image and (b) EDXS spectra of the nano HA powder

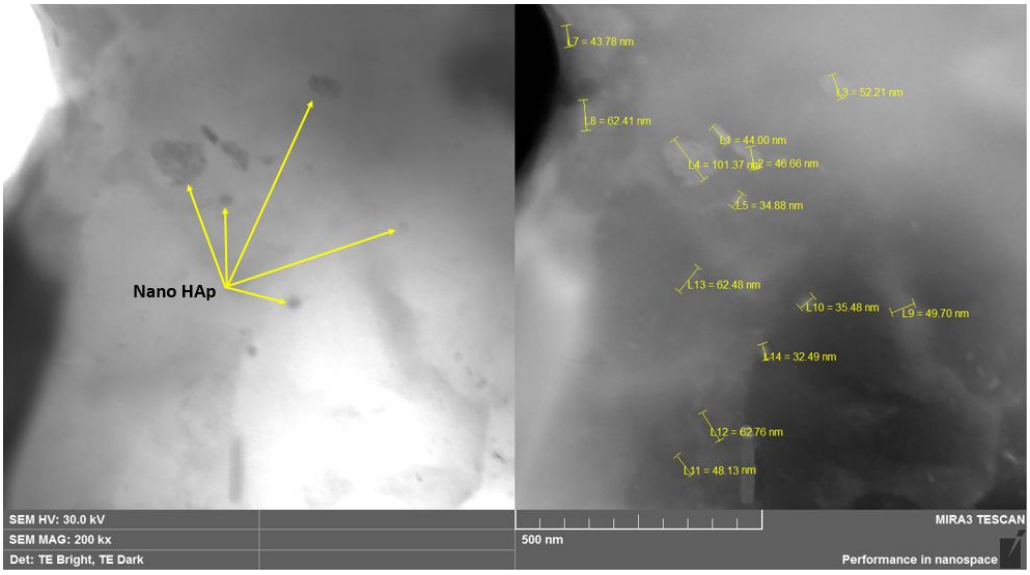

Figure 6: S-TEM images of nano HA particles

The agglomeration of nano-sized particles significantly affects the particle size evaluation. To some extent agglomeration of nano-particles are inevitable, which requires careful analysis to distinguish agglomeration of particles. For this purpose, multiple samples were carefully analyzed to obtain accurate information on particle size from the S-TEM observation. The representative S-TEM micrographs are shown in Fig. 6. (on the left side TE Bright mode – on the right side TE dark mode). S-TEM micrographs showed that particle sizes ranged from 32 nm up to 102 nm. The average particle size estimated from TEM analysis was ≈ 52 nm for 144 h ball milled at 300 rpm.

4. Conclusion

The nano hydroxyapatite powder obtained from natural supplies (human teeth) was produced as nano powder with a great success by calcination without compaction. The major phase of the calcined powder washydroxyapatite. In addition, depending on the calcination temperature, small amount of α-TCP or β-TCP phases which help osseointegration in the structure were observed. The characteristic bands of the OH^-, PO_4^{3-} and CO_3^{2-}which belongs to HA were detected from FT-IR spectra. S-TEM micrographs showed that HA particles were at ≈52 nm in average. Results indicated that it is possible to obtain nano HA particles with desired properties economically, which is suitable to be used as a graft material or tooth substitute.

Acknowledgments

My special thanks to Mr.Dr. Ali ÖZER of the Advanced Technology Research and Application Center in Cumhuriyet University for the assistance in the preparation and characterization of samples in FE-SEM.

References

1. Pepla, E., Besharat, L. K., Palaia, G., Tenore, G. & Migliau, G. (2014). Nano-Hydroxyapatite and Its Applications in Preventive, Restorative and Regenerative Dentistry: a Review of Literature. *Ann stomatal (Roma)*, 5(3):108-114.
2. Oktar F.N., Karaçaylı U. & Gündüz O. (2008). Effect of Sintering Temperature on Mechanical Properties and Microstructure of Sheep-Bone Derived Hydroxyapatite (SHA). *IFMBE Proceedings, 13th International Conference on Biomedical Engineering*. Kuala Lumpur, Malaysia, 1:147–150.
3. Kothapalli, C., Wei, M., Vasiliev, A., & Shaw, M. (2004). Influence of Temperature and Concentration on the Sintering Behavior and Mechanical Properties of Hydroxyapatite. *Acta Materialia*, 52:5655-5663.
4. Yusoff, A.H.M., Salimi, M.N. & Jamlos, M.F. (2017). Synthesis of Superparamagnetic Hydroxyapatite Core-Shell Nanostructure by a Rapid Sol-Gel Route. e-*Journal of Surface Science and Nanotechnology*, 15:121-126.
5. Lim, G.K., Wang, J.S.C., Ng. & Gan, L.M. (1999). Formation of Nanocrystalline Hydroxyapatite in Nonionic Surfactant Emulsions. *Langmuir*, 15:7472–7477.
6. Kim, W., Zhang, Q.W. & Saito, F. (2000). Mechanochemical Synthesis of Hydroxyapatite from $Ca(OH)_2$–P_2O_5 and CaO–$Ca(OH)_2$–P_2O_5 Mixtures. *Journal of Material Science*, 35:5401–5405.
7. Ooi, C.Y., Hamdi, M. & Ramesh, S. (2007). Properties of Hydroxyapatite Produced by Annealing of Bovine Bone. *Ceramic International*, 33:1171-1177.
8. Balazsi, C., Weber, F., Kover, Z., Horvath, E. & Nemeth, C. (2007). Preparation of calcium–phosphate Bioceramics from Natural Resources. *Journal of European Ceramic Society*, 27:1601-1606.
9. Yelten, A., Yilmaz, S. & Oktar, F.N. (2012). Sol–gel Derived Alumina–Hydroxyapatite–Tricalcium Phosphate Porous Composite Powders.*Ceramics International*, 38: 2659-2665.
10. Yin, M.Z., Han, Y.C., Dai, H.L. & Li, S.P. (2006). Effects of Antihepatocarcinoma with Apatite Nanoparticles *in vivo*. *Journal of Wuhan University of Technology*, 21:102–104.
11. Laquerriere, P., Grandjean-Laquerrier, A., Jallot, E., Balossier, G., Frayssinet, P. & Guenounou, M. (2003). Importance of Hydroxyapatite Particles Characteristics on Cytokines Production by Human Monocytes in vitro. *Biomaterials*, 24:2739–2747.
12. Fratzl, P., Gupta, H.S., Paschalis, E.P. & Roschger, P. (2004). Structure and Mechanical Quality of the Collagen-Mineral Nano-Composite in Bone. *Journal of Materials Chemistry*, 14: 2115–2123.
13. Kim, H.M. (2003). Ceramic Bioactivity and Related Biomimetic Strategy. *Current Opinion* in *Solid State* & *Materials Science*, 7:289–299.
14. Hench, L.L. (1998). Bioceramics, *Journal of American Ceramic Society*, 81: 1705–1728.
15. Mote, V. D., Purushotham, Y., & Dole, B.N. (2012). Williamson-Hall analysis in estimation of lattice strain in nanometer-sized ZnO particles. *Journalof Theoretical and Applied Physics*, 6:1-8.
16. Ou, S.F., Chiou, S., & Ou, K.L. (2013). Phase Transformation on Hydroxyapatite Decomposition. *Ceramics International*, 39(4): 3809-3816.
17. Zhao, J., Z. Junjie., Chen J., Wang X., Han Z. & Li, Y. (2014). Rietveld Refinement of Hydroxyapatite, Tricalcium Phosphate and Biphasic Materials Prepared by Solution Combustion Method. *Ceramics International*, 40(2):3379-3388.
18. Mishra, V.K., Bhattacharjee, B. N., Kumar, D., Rai, S.B. & Parkash, O. (2016). Effect of a Chelating Agent at Different pH on the Spectroscopic and Structural Properties of Microwave Derived Hydroxyapatite Nanoparticles: a Bone Mimetic Material. *New Journal of Chemistry*, 1(3):1- 11.
19. Abidi, S.S.A. & Murtaza, Q. (2014). Synthesis and Characterization of Nano-hydroxyapatite Powder Using Wet Chemical Precipitation Reaction. *Journal of Materials Science and Technology*, 30:307-310.